

# Deep Eutectic Solvent-Induced Polyacrylonitrile-Derived Hierarchical Porous Carbon for Zinc-Ion Hybrid Supercapacitors

Chaojie Chen<sup>+</sup>,<sup>[a]</sup> Zhiwei Li<sup>+</sup>,<sup>[a]</sup> Yinghong Xu,<sup>[a]</sup> Haojie Liao,<sup>[a]</sup> Langyuan Wu,<sup>[a]</sup> Hui Dou,<sup>[a]</sup> and Xiaogang Zhang<sup>\*[a]</sup>

Hierarchical porous carbon that possesses large surface area and high porosity has become an important electrode material for supercapacitors. However, some unavoidable issues like complex approach and environmental pollution involved in traditional chemical activation restrict the sustainable development of carbons. Herein, a green, low-cost, and safe urea-zinc chloride deep eutectic solvent (DES) is proposed to prepare polyacrylonitrile derived three-dimensional carbon nanosphere (D-PC). Specially, the D-PC efficiently accelerates electrolyte ions migration and enhances charge storage due to its interconnected ionic pathways and large accessible active surfaces.

When employing the D-PC as positive electrode of zinc-ion hybrid supercapacitors, a high specific capacitance of  $261.5 \text{ F g}^{-1}$  at  $0.2 \text{ A g}^{-1}$  along with a cycling stability of 91.3% after 10000 cycles at  $5 \text{ A g}^{-1}$ . Meanwhile, such device holds the maximum energy/power density of  $93.9 \text{ Wh kg}^{-1}/16.7 \text{ kW kg}^{-1}$  at  $0.2 \text{ A g}^{-1}/20 \text{ A g}^{-1}$ , respectively. Thanks to the unique physicochemical properties of as-obtained D-PC, an ultrahigh areal capacitance of  $2.2 \text{ F cm}^{-2}$  also can be achieved at a mass loading of  $23 \text{ mg cm}^{-2}$ . The satisfying structure and performance highlight the potential of DESs in the design of functional carbons.

## 1. Introduction

The ever-increasing demand of electrical market has triggered continuous attention into rechargeable devices with high safety, cost-effectiveness, environmental friendliness.<sup>[1]</sup> Although Lithium ion batteries (LIBs) have been regarded as one of the most promising systems for energy storage, the relatively poor power output ( $< 5000 \text{ W kg}^{-1}$ ) and questionable safety issue are greatly limit their application.<sup>[2]</sup> Therefore, the development and pursuit of alternatives has become an urgent priority yet a challenge.

In recent years, various metallic ion supercapacitors have been designed and constructed.<sup>[3]</sup> Typically, a hybrid supercapacitor (HSC) contains a battery-type negative electrode, a capacitor-like positive electrode, and matched electrolyte.<sup>[4]</sup> Based on this combination, both high power and energy density could be achieved.<sup>[5]</sup> When considering the safety issues and environmental concerns caused by the flammable organic electrolytes, the re-emerged aqueous devices may be appropriate for large-scale energy storage.<sup>[6]</sup> Taking aqueous hybrid supercapacitors (HSCs) as an example, zinc-based SCs (ZHSCs)

are greatly attractive and promising due to the unique properties of Zn electrode, namely, low redox potential of  $\text{Zn/Zn}^{2+}$  ( $-0.76 \text{ V}$  vs. the standard hydrogen electrode), high theoretical capacity ( $820 \text{ mAh g}^{-1}/5851 \text{ mAh cm}^{-3}$ ), and good water compatibility.<sup>[7]</sup> In addition, carbon-based materials are always employed as promising positive electrodes thanks to their high electroactive surface area, industrial production, and favorably physicochemical features.<sup>[8]</sup> For instance, Liu and Lu et al. developed a high-performance ZHSC based on a nitrogen-doped porous carbon by hard template, delivering a high energy density of  $107.3 \text{ Wh kg}^{-1}$  at a current density of  $4.2 \text{ A g}^{-1}$  together with a long-term stability over 20000 cycles.<sup>[9]</sup> Besides, Zhang et al. prepared a pencil shaving-delivered carbon for the construction of anti-freezing ZHSC, which achieved specific capacities of 413.3 and  $236.3 \text{ F g}^{-1}$  at the mass loading of 2 and  $24 \text{ mg cm}^{-2}$ , respectively.<sup>[10]</sup> Very recently, Zhao and Ma et al. designed N, O co-doped porous carbon by integrating Zn-zeolitic imidazolate framework (ZIF-8) and polyacrylonitrile (PAN). Consequently, a satisfying capacity of  $138.5 \text{ mAh g}^{-1}$  was delivered at  $0.5 \text{ A g}^{-1}$ , suggesting a high energy density of  $110 \text{ Wh kg}^{-1}$ .<sup>[11]</sup> It is worth noting that *N,N*-dimethylformamide (DMF) always employs as an appropriate solvent to disperse PAN based on the rule of the likes dissolve each other.<sup>[12]</sup> Nevertheless, the toxicity and complexity involved in this process are the key issues that limit practical applications of such materials. Therefore, the development of green and low-cost solvent for the preparation of PAN-based porous carbon still is an imperative task in the near future.

Deep eutectic solvents (DESs), as one of new ionic liquids, are widely applied in energy-related areas due to their unique properties including low cost, environmental friendliness and biodegradability.<sup>[13]</sup> Typically, the DES is formed by the

[a] C. Chen,<sup>+</sup> Z. Li,<sup>+</sup> Y. Xu, H. Liao, L. Wu, Prof. H. Dou, Prof. X. Zhang  
Jiangsu Key Laboratory of Electrochemical Energy Storage Technologies  
College of Material Science and Technology  
Nanjing University of Aeronautics and Astronautics  
Nanjing 211106, P. R. China  
E-mail: azhangxg@nuaa.edu.cn

[+] These authors contributed equally to this work.

 Supporting information for this article is available on the WWW under  
<https://doi.org/10.1002/batt.202000250>

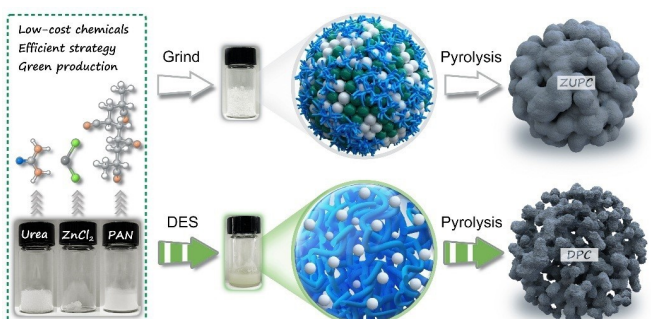
 An invited contribution to a Special Collection dedicated to Metal-Ion Hybrid Supercapacitors

coordination of hydrogen bond donor (HBD) and hydrogen bond acceptor (HBA). Comparing with the melting point of each component, the charge delocalization between HBD and HBA can significantly decrease the freezing point of such mixture. According to this view, DESs are rationally used to recycle or extract valuable elements from the cathode materials of lithium-ion batteries.<sup>[14]</sup> Owing to the convenient composition of DES, various functional solvents can be obtained only by adjusting the type of HBD and HBA, which may be a favor strategy to engineer promising materials for energy storage. However, the potential of DESs to induce the structure of functional carbons (especially polymer-based carbon) has not been greatly explored.

Herein, we demonstrated the employment of PAN and DESs as carbonaceous precursors and pore-engineering agents for preparation of the hierarchical porous carbon (D-PC). The DESs selected were formed by using urea and zinc chloride ( $ZnCl_2$ ) with a molar ratio of 7:1, in which urea could result in the heteroatom doping and  $ZnCl_2$  may function as activation agent to create pores. Thanks to the high hydrogen bond accept ability of cyano group (-CN), the PAN can act as one of HBAs to participate the formation of continuous hydrogen network, benefitting the complete dispersion of PAN as well as the formation of high porosity. The as-prepared D-PC exhibits a good energy storage behavior owing to its large specific surface area, hierarchical porosity, and N, O co-doping. Combined by the physical/chemical adsorption/desorption processes, the D-PC based ZHSC delivers a high specific capacitance of  $261.5 \text{ F g}^{-1}$  at a current density of  $0.2 \text{ A g}^{-1}$  and remains superior durability with 8.7% capacitance loss over 10000 cycles at  $5 \text{ A g}^{-1}$ . Meanwhile, a high areal capacitance of  $2.2 \text{ F cm}^{-2}$  can be achieved at a high mass loading of  $23 \text{ mg cm}^{-2}$ .

## 2. Results and Discussion

The preparation for porous carbon under various approaches is illustrated in Scheme 1. As shown, the D-PC was synthesized by a unique DES-assisted strategy using PAN as the carbon source. Urea and  $ZnCl_2$  were employed as the dopant and activator, respectively. Notably, the employed urea and  $ZnCl_2$  can form a hydrogen bond induced solution (Figure S1), which would



Scheme 1. Schematic illustration of the preparation of ZU-PC and D-PC.

disperse PAN uniformly in stretched chains rather than clusters. As observed, such DES shows a transparent nature (Figure S2a), while the solution becomes milky with the addition of PAN (Figure S2b) in few second without any agglomerated particles exhibited. In this view, we can conclude that as-prepared DES is one type of dispersants of PAN. When taking a consideration of the activation effect of Zn-based salts under high pyrolyzed temperature, such mixture with DES was further converted into porosity-rich carbon than that with common grind process (ZU-PC).

The microstructures of as-obtained carbons were characterized by field-emission scanning electron microscope (FESEM) and transmission electron microscope (TEM), as shown in Figure 1. SEM images of the PC at different magnifications hold a ball-like structure with a relatively smooth surface (Figure 1a and b). Meanwhile, no obvious pores are found in the PC sample by TEM (Figure 1c). As a strong contrast, the D-PC shows the well-developed hierarchical porous structure (Figure 1d-f), which mainly caused by the synergic effect between PAN and DES. From the high-resolution TEM image of the D-PC (Figure 1g), numerous nanopores are observed in the nanosheets, which suggests a relatively large specific surface area (SSA) and high pore volume for energy storage. Moreover, the presentation of two diffraction rings detected by the selected area electron diffraction (SAED) further confirms the amorphous nature of as-prepared D-PC (Figure S3). In contrast to other carbons like the ZU-PC, U-PC, and Z-PC (Figure S4), the D-PC carbon displays relatively uniform size and interconnected porosity. Besides, the energy dispersive X-ray analysis (EDX) demonstrates that the D-PC is evenly composed by the C, N, and O elements (Figure 1h and S5), indicating the thoroughly removal of impurities. The signal for Cu presented in Figure S5 is mainly attributed to the employed Cu mesh substrate during TEM observation. As known, the heteroatoms doping can not only improve the wettability of carbons, but also provide a plenty of active sites. Combining with the hierarchical microstructure, such carbon may deliver satisfying electrochemical performance.

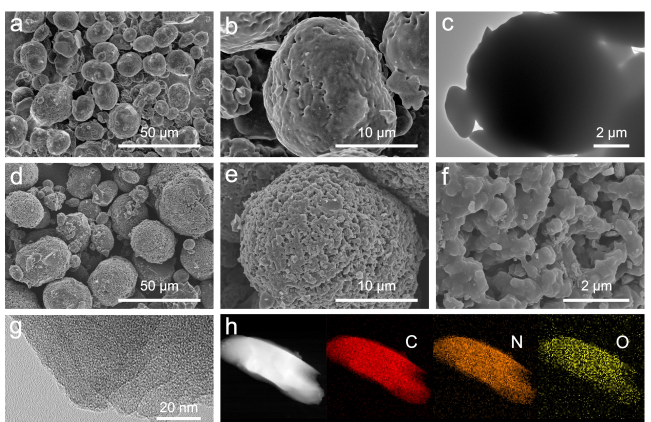


Figure 1. a, b) SEM images, c) TEM image of the PC. d-f) SEM images, g) HRTEM image, and h) element mappings of the D-PC.

To further gain insight into the structure of carbons obtained,  $N_2$  adsorption and desorption tests were conducted for as-prepared products at 77 K. As shown in Figure 2a, D-PC, ZU-PC, and Z-PC possess the characteristic of type I isotherm. It is worth mentioning that the rapid increase of adsorbed quantity at the low relative pressure for these carbons suggests the existence of abundant micropores. However, the ultralow adsorption behavior of the U-PC and PC at each relative pressure region means their relatively poor pore structure. According to the Brunauer-Emmett-Teller (BET) method, the SSA can be gradually increasing from  $3.1\text{ m}^2\text{ g}^{-1}$  (PC) to  $852\text{ m}^2\text{ g}^{-1}$  (D-PC) by employing the DES strategy (Figure S6). Based on the non-linear density functional theory (NLDFT), the pore size distribution of various carbon shows remarkable differences (Figure 2b). For the D-PC, the pore sizes are mainly centered at 0.6, 0.8, 1.1, 1.3, 1.4, 1.6, and 1.9 nm, indicating the hierarchical porous feature. Comparably, the pores for ZU-PC and Z-PC are located at 0.6, 0.8, 1.1, and 1.4 nm, while the PC and U-PC samples show no pore distribution. Such hierarchical porous structure of D-PC carbon is highly expected to achieve a favorable electrochemical performance with improved ions diffusion/rapid kinetics. X-ray powder diffraction (XRD) patterns and Raman spectra were typically used to investigate the crystal structure and disordered degree of formed carbons. As profiled in Figure 2c, the XRD patterns display two broaden diffraction peaks at  $24.3^\circ$  and  $43.6^\circ$ , which can be corresponding to the typical (002) and (100) planes of graphite.<sup>[10]</sup> Notably, the (002) planes of D-PC, ZU-PC, Z-PC, and U-PC slightly shift to the lower angle region when comparing with the PC. This phenomenon suggests that such samples have a relatively larger inner space than PC. To further study the structural change and graphitization degree, Raman spectra for various carbons were conducted (Figure 2d). Two characteristic peaks located at  $1338\text{ cm}^{-1}$  (D band) and  $1586\text{ cm}^{-1}$  (G band) are

related to the defects and the graphitic carbons. Generally, the calculated  $I_D/I_G$  value is an effective indicator to evaluate the density of defects.<sup>[7c]</sup> The higher  $I_D/I_G$  ratio of D-PC (0.992), ZU-PC (1.072), Z-PC (1.425), and U-PC (1.042) than PC (0.991), implying more defects or disordered regions in carbons with  $ZnCl_2$  or urea induced by the chemical interactions during pyrolysis.

X-ray photoelectron spectroscope (XPS) was performed to study the chemical composition and the bond state of as-prepared D-PC. As depicted in Figure S7, C, N, and O elements located at 284.8, 399.8 and 531.8 eV are detected in XPS spectrum, confirming the successful doping of heteroatoms. In addition, the content of N and O is 12.14 and 7.62 at% respectively. Specifically, four peaks are divided from the high-resolution N 1s spectrum, which can be assigned to the pyridine N (N-6, 398.5 eV, 36.1%), pyrrolic N (N-5, 399.9 eV, 24.4%), graphitic N (N-Q, 400.8 eV, 32.0%), and oxidized N (N-X, 404.4 eV, 7.5%), respectively.<sup>[15]</sup> Meanwhile, the high-resolution O 1s spectrum exhibits three types of oxygen groups, which includes O-I ( $C=O$ , 531.7 eV, 57.5%), O-II ( $C-OH$ / $C-O-C$ , 532.6 eV, 26.4%) and O-III ( $-COOH$ , 533.7 eV, 16.1%).<sup>[16]</sup> To our knowledge, the nitrogen and oxygen groups can not only provide abundant active sites, but also enhance the charge storage by introducing extra pseudocapacitance. Taking a comprehensive consideration, the DES-assisted carbon may deliver promising performances, especially for energy storage due to its large SSA, hierarchical porosity, and heteroatoms doping.

In order to evaluate the electrochemical performances of prepared samples, we constructed ZHSCs by using as-prepared carbons as the positive electrode and Zn foil as the negative electrode in  $1\text{ mol L}^{-1}$   $ZnSO_4$ . The mass loading of active materials on positive electrode is typically about  $1.8\text{ mg cm}^{-2}$  unless otherwise specified. Cyclic voltammetry (CV) curves of

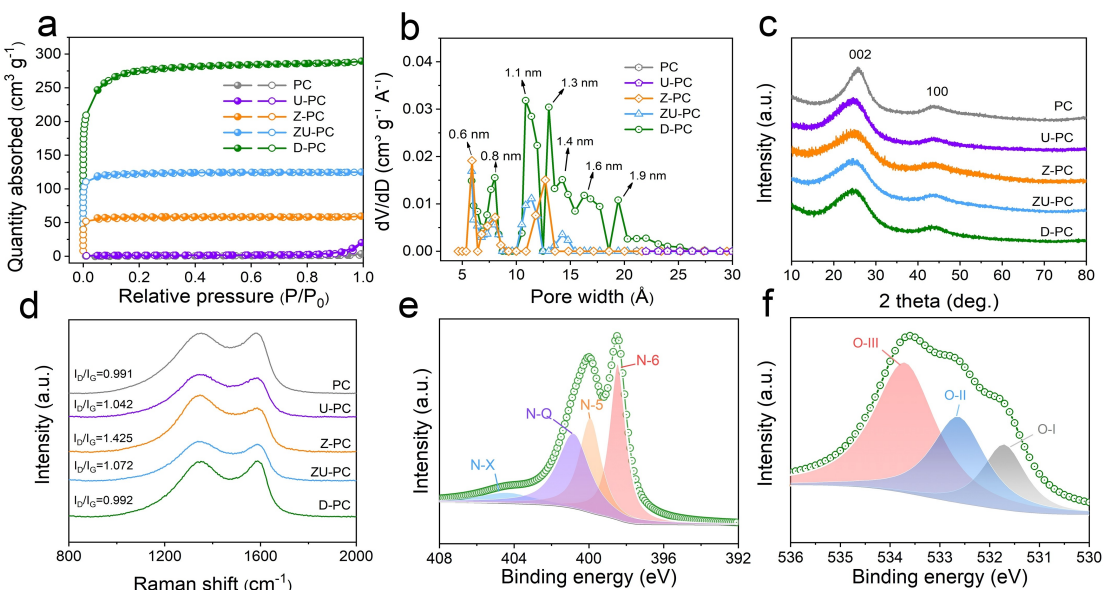


**Figure 2.** a)  $N_2$  absorption/desorption isotherms, b) pore sizes distribution, c) XRD patterns, d) Raman spectra for various carbons. High-resolution e) N 1s and f) O 1s spectra for the D-PC.

the Zn and the D-PC electrodes indicate that a wide voltage range (1.8 V) can be achieved. As shown in Figure 3a, the sharp redox peaks at about  $-1.2/-0.91$  V (vs. SCE) can be ascribed to the plating and stripping of Zn electrode.<sup>[17]</sup> For the D-PC electrode, a rectangular-like shape can be obtained, revealing its ideal capacitive behaviors. As expected, the D-PC-based ZHSC (Zn//D-PC) displays the highest enclosed area among other devices (Figure 3b), which means the highest charge storage capability. It needs to point out that the weak redox peaks at around 0.6/1.2 V suggest the existence of pseudocapacitance induced by the functional groups besides dominated ions adsorption/desorption. The galvanostatic charge/discharge (GCD) curves at  $0.2 \text{ A g}^{-1}$  (Figure 3c) further demonstrate that the good reversibility and satisfying capacitance. In addition, the relatively low IR drop of the Zn//D-PC ( $0.018 \text{ V}$ ) compared with Zn//ZU-PC ( $0.127 \text{ V}$ ), Zn//Z-PC ( $0.110 \text{ V}$ ), Zn//U-PC ( $0.118 \text{ V}$ ), Zn//PC ( $0.169 \text{ V}$ ), and Zn//YP-50F ( $0.033 \text{ V}$ ) proves that the moderate heteroatoms doping and defects density is capable of effectively modifying the interface property (especially the wettability) (Figure S8).<sup>[10]</sup> Accordingly, the specific capacitance of the Zn//D-PC invariably surpasses that of other assembled devices under various current densities from  $0.2$  to  $20 \text{ A g}^{-1}$  (Figure 3d). As profiled, a high capacitance of  $261.5$  and  $145.8 \text{ F g}^{-1}$  can be achieved at  $0.2$  and  $20 \text{ A g}^{-1}$ , respec-

tively, which is higher than that of Zn//YP-50F ( $145 \text{ F g}^{-1}$ ) and those of other devices built (Figure 3d). Note that the capacitance of  $260.1 \text{ F g}^{-1}$  can return with the current density back to  $0.2 \text{ A g}^{-1}$ , indicating the outstanding electrochemical reversibility. Notably, the similar capacitance values of the YP-50F at the closed current densities ( $0.8$  and  $1 \text{ A g}^{-1}$ ) mainly are mainly due to the similar concentration polarization near the interfaces between electrode and electrolyte and sluggish response to electrochemical signals caused by micropores. Furthermore, the energy density and power density of as-fabricated ZHSCs and other previously reported devices are summarized and profiled in Figure 3e. The Zn//D-PC can deliver the highest power density of  $16.7 \text{ kW kg}^{-1}$  at a energy density of  $51 \text{ Wh kg}^{-1}$ , and the maximum energy density of  $93.9 \text{ Wh kg}^{-1}$  at an power density of  $163.9 \text{ W kg}^{-1}$ , which are higher than that of Zn//ZU-PC ( $57.6 \text{ Wh kg}^{-1}$ ,  $4.1 \text{ kW kg}^{-1}$ ), Zn//Z-PC ( $46.6 \text{ Wh kg}^{-1}$ ,  $0.8 \text{ kW kg}^{-1}$ ), Zn//U-PC ( $19.4 \text{ Wh kg}^{-1}$ ,  $0.9 \text{ kW kg}^{-1}$ ), Zn//PC ( $6.9 \text{ Wh kg}^{-1}$ ,  $0.6 \text{ kW kg}^{-1}$ ), and Zn//YP-50F ( $55.1 \text{ Wh kg}^{-1}$ ,  $6.2 \text{ kW kg}^{-1}$ ). To a literature survey, such results are very comparable even superior to some of other reported ZHSCs, including Zn//LDC ( $86.8 \text{ Wh kg}^{-1}$ ,  $12.2 \text{ kW kg}^{-1}$ ),<sup>[8a]</sup> Zn//AC ( $52.7 \text{ Wh kg}^{-1}$ ,  $1.7 \text{ kW kg}^{-1}$ ),<sup>[18]</sup> Zn//ZnHCF ( $100 \text{ Wh kg}^{-1}$ ,  $1.7 \text{ kW kg}^{-1}$ ),<sup>[19]</sup> Zn//HCS, ( $59.7 \text{ Wh kg}^{-1}$ ),<sup>[20]</sup> MnO<sub>2</sub>@CAC//MXene@COC ( $90 \text{ Wh kg}^{-1}$ ,  $3.8 \text{ kW kg}^{-1}$ ).<sup>[21]</sup> Moreover, an extremely

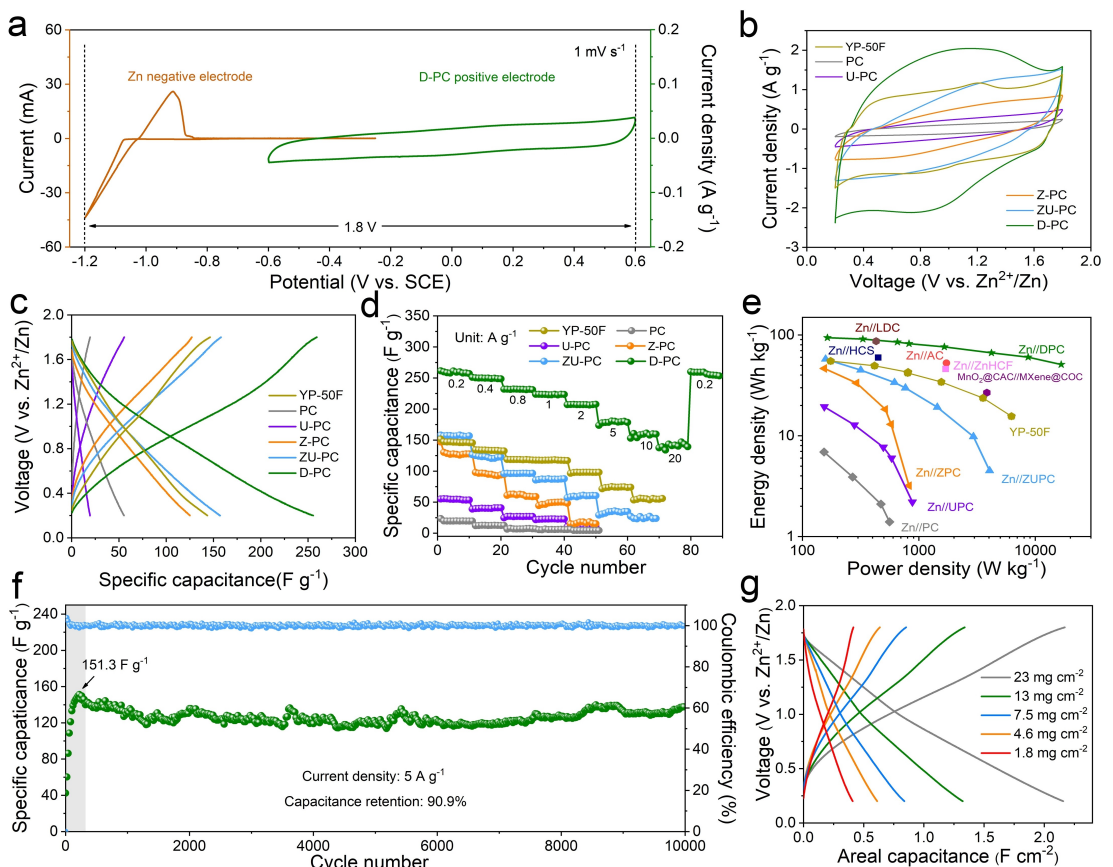


**Figure 3.** a) CV curves of the Zn and D-PC electrodes tested at a scan rate of  $1 \text{ mV s}^{-1}$ . b) CV curves at  $10 \text{ mV s}^{-1}$ , c) GCD curves at  $0.2 \text{ A g}^{-1}$ , and d) rate performances of various electrodes. e) Comparison of Zn//D-PC devices with other aqueous ZHSCs. f) Cycling stability of the D-PC at a current density of  $5 \text{ A g}^{-1}$  over 10000 cycles. g) GCD curves of the D-PC with different mass loading.

excellent durability with about 91 % capacitance retention over 10000 cycles at a current density of  $5 \text{ A g}^{-1}$  was also performed (Figure 3f). Notably, the gradually increase occurred in the initial cycling test mainly results from the electrochemical activation.<sup>[22]</sup> Besides, the TEM images observed after cycling test shows the porous nature of D-PC, further confirming the satisfied durability of as-optimized D-PC electrode (Figure S9). As is well known, the development of advanced electrode with high mass loading is greatly essential to the construction of miniaturized electronics.<sup>[23]</sup> However, the unsatisfying pore structure or ultrahigh surface area of activated carbons always block their application due to the sluggish kinetics or poor wettability. Inspired by the unique physicochemical properties of the D-PC, we have prepared and measured a series of electrodes with different mass loading from 1.8 to 23 mg cm<sup>-2</sup>. ~43.8% of the specific capacitance still can be remained even with the increase of mass loading from 1.8 to 23 mg cm<sup>-2</sup>, denoting a relatively high areal capacitance of  $2.2 \text{ F cm}^{-2}$  (Figure 3g).

To further study the kinetics of such ZHSCs, electrochemical impedance spectra (EIS) were conducted in a frequency ranging from 0.01 Hz to 100 kHz (Figure 4a). Typically, the semicircle in the high frequency is corresponding to the charge transfer resistance ( $R_{ct}$ ) on the electrode. And the slanted line in the low frequency represents the diffusion of electrolytes ions

( $Z_w$ ).<sup>[24]</sup> Apparently, through data fitting, the D-PC shows fast charge transfer as well as ions diffusion when compared to the PC (Figure 4b). Meanwhile, a typical model was employed to study the capacitance effects over the whole frequency range, as illustrated by Equations (1)–(4):

$$C(\omega) = C'(\omega) + jC''(\omega) \quad (1)$$

$$C'(\omega) = \frac{-Z'(\omega)}{\omega|Z(\omega)|^2} \quad (2)$$

$$C''(\omega) = \frac{Z'(\omega)}{\omega|Z(\omega)|^2} \quad (3)$$

$$\omega = 2\pi f \quad (4)$$

In this view, the capacitance at various frequency can be divided into the real part ( $C'(\omega)$ ) and the imaginary part ( $C''(\omega)$ ) from EIS data. As plotted in Figure 4c, d, a dramatical increase of  $C'$  values can be found in the low frequency region ( $f < 1 \text{ Hz}$ ), delivering a high longitudinal intercept of  $0.064 \text{ F cm}^{-2}$ . Meanwhile, the  $C''$  value corresponded to the irreversible processes during electrochemical tests proves the satisfying properties of D-PC compared to that of the PC. As profiled in Figure 4e, the Zn//D-PC holds the rectangular-like shape at various scan rates

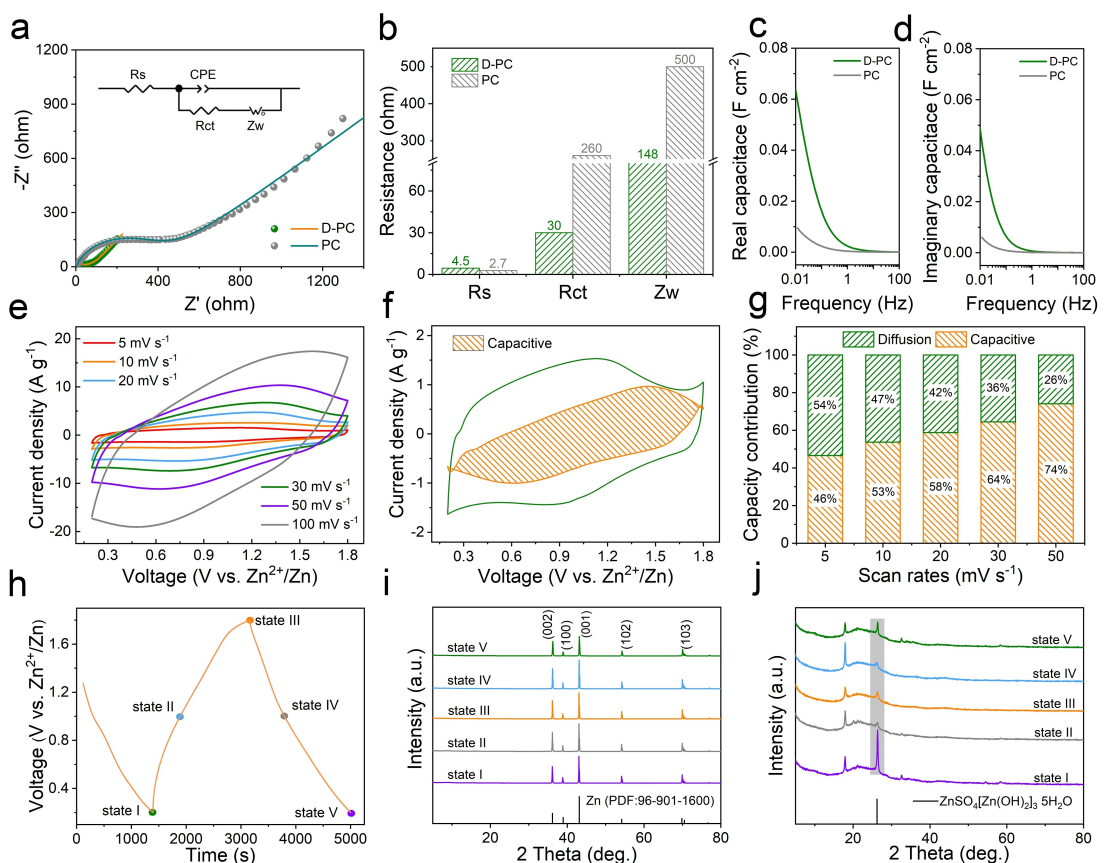
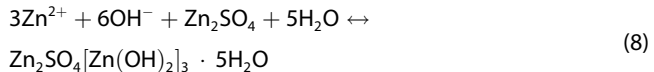


**Figure 4.** a) Nyquist plots, b) comparisons of  $R_s$ ,  $R_{ct}$  and  $Z_w$  values, c) real capacitance and d) imaginary capacitance of D-PC and PC. e) CV curves at various scan rates, f) separation of diffusion contribution and capacitive contribution at  $5 \text{ mV s}^{-1}$ , and g) capacitive contribution ( $k_1 v$ ) and diffusion contribution ( $k_2 v^{1/2}$ ) at various scan rates for Zn//D-PC. Ex-situ XRD patterns recorded h) at various charge-discharge states at  $0.2 \text{ A g}^{-1}$  for i) Zn electrodes and j) D-PC electrodes.

from 5 to 100 mVs<sup>-1</sup>, suggesting good electrochemical behavior. To our knowledge, the contributions of capacitance for as-constructed ZHSCs are rationally analyzed by the CV curves according to the Dunn's method ( $i = k_1v + k_2v^{1/2}$ ).<sup>[22]</sup> Typically, the values of  $k_1v$  and  $k_2v^{1/2}$  are related to the capacitive contribution and diffusion-controlled contribution. As a result, a relatively high capacitive contribution of ~46% is calculated at the scan rate of 5 mVs<sup>-1</sup> (Figure 4f). Besides, the proportion of capacitance contribution gradually enlarges to 74% with the increasement of scan rates (from 5 to 50 mVs<sup>-1</sup>), demonstrating the dominant role of capacitance in the whole energy storage process (Figure 4g).<sup>[25]</sup>

Although the Zn//D-PC device delivers several favorable performances based on above discussion, the relevant operating mechanism is still controversial. To further study and clarify the detail charge storage procedure of such ZHSCs, we have conducted *ex-situ* XRD measurements under various states of charge/discharge (Figure 4h). Owing to the satisfying plating/stripping of Zn electrode, each electrode remains the characteristic peaks corresponded to the Zn metal without any other impurities, revealing its good reversibility.<sup>[26]</sup> It is worth noting that the D-PC electrodes present two obvious peaks, which could be the characteristic peaks of PTFE (17.9°) and Zn<sub>2</sub>SO<sub>4</sub>[Zn(OH)<sub>2</sub>]<sub>3</sub>·5H<sub>2</sub>O (26.4°).<sup>[10,27]</sup> Yet, the produced Zn<sub>2</sub>SO<sub>4</sub>[Zn(OH)<sub>2</sub>]<sub>3</sub>·5H<sub>2</sub>O can induce a highly reversible formation/dissolution along with the repeated charging and discharging, in line with some previous reports.<sup>[26,27]</sup> At the same time, the location and intensity of broad (002) plane does not change, further confirming the governed adsorption/desorption of electrolyte ions. Based on the analyses, the possible charge storage processes and faradaic redox reactions for the oxygen groups can be proposed as follows [Eqs. (5)–(9)].<sup>[16,9,18]</sup>

#### Positive electrode:



#### Negative electrode:



### 3. Conclusions

In summary, we have successfully demonstrated the potential of DES in the design of hierarchical porous carbon as both solvent and template. The *in-situ* activation of zinc-based salt in selected DES enables the favorable porous structure. The urea contained in as-formed DES can play a role of heteroatom doping. Consequently, the as-obtained D-PC exhibits large electroactive surface area, high porosity and N/O co-doped feature. More importantly, such Zn//D-PC device displays a

high specific capacitance (296.78 F g<sup>-1</sup> at 0.2 A g<sup>-1</sup>) and satisfying durability (~137.5 F g<sup>-1</sup> over 10000 cycles at 5 A g<sup>-1</sup>). In addition, a relatively high capacitance retention of ~44% can be achieved even under a high mass loading of 23 mg cm<sup>-2</sup>. According to this finding, we believe that the proposed strategy is very promising for sustainable carbon preparation as well as scalable energy storage.

## Experimental Section

### Chemicals

All chemical reagents were of analytical grade and obtained commercially. The PAN ( $M_w$ : ~150000) was purchased from Macklin Biochemical Co., Ltd. (Shanghai, China). Urea was obtained from Aladdin Chemical Co., Ltd. (Shanghai, China). ZnCl<sub>2</sub> and ZnSO<sub>4</sub>·7H<sub>2</sub>O were provided by Nanjing Chemical Reagent Co., Ltd. (Nanjing, China).

### Synthesis of DES-assisted porous carbon

Typically, 0.75 g of PAN was dispersed in as-formed DES solution under vigorous stirring. It is worth mentioning that the DES was prepared by mixing zinc chloride (ZnCl<sub>2</sub>) and urea according to a molar ratio of 1:7 under continuous stirring at 70°C. After then, the mixture was pyrolyzed at 800°C for 2 h together with a stabilized process at 350°C for 1 h under nitrogen flow. The porous carbon assisted by DES (D-PC) was obtained after purifying by diluted hydrochloric acid and deionized water and drying at 60°C. For comparison, a series of porous carbon materials (PC, U-PC, Z-PC, and ZU-PC) with various components (Table S1) were also prepared by the same conditions.

### Characterization

The structure and morphology of samples were characterized by XRD (PANalytical Empyrean, Holland), Raman spectroscopy (Horiba Scientific LabRAM HR, France), and FESEM (Hitachi S-4800, Japan) as well as a HRTEM (JEOL JEM-2100, Japan). The SSA and pore size distribution of carbons were analyzed by applying BET method and NLDFT model with ad-/desorption instrument (Micromeritics ASAP 2460, USA). The surface chemistry was measured by using XPS (KRATOS AXIS SUPRA, Japan).

### Electrochemical Measurements

Carbon electrodes were prepared by casting a rolled and punched film of 80 wt% carbon materials, 10 wt% acetylene black, and 10 wt% PTFE on graphite current collector and dried at 60°C. The mass loading of each electrode was about 1.8~23 mg cm<sup>-2</sup>. All the electrochemical performances of as-obtained working electrodes were tested by CR2016 coin cells, which assembled with polished Zn (thickness: 80 μm) as the counter electrode, Whatman filter (CAT NO. 1005-05) as the separator, 1 mol L<sup>-1</sup> ZnSO<sub>4</sub> aqueous solution as the electrolyte. LAND CT 2001 A system was used to test GCD curves and cycling stability between 0.2 and 1.8 V (vs. Zn<sup>2+</sup>/Zn). CHI 760E (Chenhua, Shanghai) electrochemical working station was employed to operate CV curves and EIS spectra at a constant room temperature of 25°C. In addition, the areal capacitance ( $C_a$ , F cm<sup>-2</sup>) and power density ( $P$ , W kg<sup>-1</sup>) were calculated by Equations (10) and (11):

$$C_a = m C_m \quad (10)$$

$$P = 3600 \times \frac{E}{\Delta t} \quad (11)$$

where  $E$  (Wh kg<sup>-1</sup>) is obtained from LAND system directly,  $C_m$  (F g<sup>-1</sup>) represents the specific capacitance of discharging part,  $\Delta V$  (V) is the working voltage, and  $\Delta t$  (s) is the discharging time.

## Acknowledgements

This work is supported by the National Natural Science Foundation of China (U1802256, 21773118, 21875107, 52072173), the Key Research and Development Program in Jiangsu Province (BE2018122), and a Project Funded by the Priority Academic Program Development of Jiangsu Higher Education Institutions (PAPD).

## Conflict of Interest

The authors declare no conflict of interest.

**Keywords:** hierarchical porous carbon · deep eutectic solvent · polyacrylonitrile · zinc-ion hybrid supercapacitors

- [1] a) J. F. Parker, C. N. Chervin, I. R. Pala, M. Machler, M. F. Burz, J. W. Long, D. R. Rolison, *Science* **2017**, *356*, 414–417; b) Q. Zhao, Z. Zhu, J. Chen, *Adv. Mater.* **2017**, *29*, 1607007; c) L. Zhou, K. Zhang, Z. Hu, Z. Tao, L. Mai, Y.-M. Kang, S.-L. Chou, J. Chen, *Adv. Energy Mater.* **2018**, *8*, 1701415; d) Y. Liang, H. Dong, D. Aurbach, Y. Yao, *Nat. Energy* **2020**, *1*, 1–11; e) X. Jia, C. Liu, Z. G. Neale, J. Yang, G. Cao, *Chem. Rev.* **2020**, *120*, 7795–7866; f) G. Sun, H. Yang, G. Zhang, J. Gao, X. Jin, Y. Zhao, L. Jiang, L. Qu, *Energy Environ. Sci.* **2018**, *11*, 3367–3374; g) G.-H. An, J. Hong, S. Pak, Y. Cho, S. Lee, B. Hou, S. Cha, *Adv. Energy Mater.* **2020**, *10*, 1902981.
- [2] a) F. Yu, C. Zhang, F. Wang, Y. Gu, P. Zhang, E. R. Wadlawik, A. Du, K. Ostríkov, H. Wang, *Mater. Horiz.* **2020**, *7*, 495–503; b) G. Zhou, F. Li, H.-M. Cheng, *Energy Environ. Sci.* **2014**, *7*, 1307–1338; c) F. Wu, J. Maier, Y. Yu, *Chem. Soc. Rev.* **2020**, *49*, 1569–1614; d) L. Wang, Z. Wu, J. Zou, P. Gao, X. Niu, H. Li, L. Chen, *Joule* **2019**, *3*, 2086–2102.
- [3] a) G. Zou, H. Hou, G. Zhao, Z. Huang, P. Ge, X. Ji, *Green Chem.* **2017**, *19*, 4622–4632; b) M. Chen, L. Wang, X. Sheng, T. Wang, J. Zhou, S. Li, X. Shen, M. Zhang, Q. Zhang, X. Yu, J. Zhu, B. Lu, *Adv. Funct. Mater.* **2020**, *30*, 2004247; c) Z. Huang, A. Chen, F. Mo, G. Liang, X. Li, Q. Yang, Y. Guo, Z. Chen, Q. Li, B. Dong, C. Zhi, *Adv. Energy Mater.* **2020**, *10*, 2001024; d) L. Dong, W. Yang, W. Yang, Y. Li, W. Wu, G. Wang, *J. Mater. Chem. A* **2019**, *7*, 13810–13832; e) Y. Zhang, J. Jiang, Y. An, L. Wu, H. Dou, J. Zhang, Y. Zhang, S. Wu, M. Dong, X. Zhang, Z. Guo, *ChemSusChem* **2020**, *13*, 2522–2539; f) Y. Cho, S. Pak, Y.-G. Lee, J. S. Hwang, P. Giraud, G.-H. An, S. Cha, *Adv. Funct. Mater.* **2020**, *30*, 1908479; g) S. Dong, Y. Wang, C. Chen, L. Shen, X. Zhang, *Nano-Micro Lett.* **2020**, *12*, 168–179.
- [4] a) J. Jiang, Y. Zhang, Y. An, L. Wu, Q. Zhu, H. Dou, X. Zhang, *Small Methods* **2019**, *3*, 1900081; b) J. Jiang, G. Nie, P. Nie, Z. Li, Z. Pan, H. Dou, X. Zhang, J. Wang, *Nano-Micro Lett.* **2020**, *12*, 1–30.
- [5] L. Wu, S. Dong, G. Pang, H. Li, C. Xu, Y. Zhang, H. Dou, X. Zhang, *J. Mater. Chem. A* **2019**, *7*, 1030–1037.
- [6] a) Z. Li, Y. An, S. Dong, C. Chen, L. Wu, Y. Sun, X. Zhang, *Energy Storage Mater.* **2020**, *31*, 252–266; b) Y. Shao, Z. Sun, Z. Tian, S. Li, G. Wu, M. Wang, X. Tong, F. Shen, Z. Xia, V. Tung, J. Sun, Y. Shao, *Adv. Funct. Mater.* **2020**, 2007843; c) Z. Li, L. Wu, S. Dong, T. Xu, S. Li, Y. An, J. Jiang, X. Zhang, *Adv. Funct. Mater.* **2020**, 2006495.
- [7] a) X. Li, M. Li, Q. Yang, D. Wang, L. Ma, G. Liang, Z. Huang, B. Dong, Q. Huang, C. Zhi, *Adv. Energy Mater.* **2020**, *14*, 541–551; b) P. Liang, J. Yi, X. Liu, K. Wu, Z. Wang, J. Cui, Y. Liu, Y. Wang, Y. Xia, J. Zhang, *Adv. Funct. Mater.* **2020**, *30*, 1908528; c) J. Yin, W. Zhang, W. Wang, N. A. Alhebsi, N. Salah, H. N. Alshareef, *Adv. Energy Mater.* **2020**, 2001705; d) Z. Wang, J. Huang, Z. Guo, X. Dong, Y. Liu, Y. Wang, Y. Xia, *Joule* **2019**, *3*, 1289–1300; e) F. Wan, Y. Zhang, L. Zhang, D. Liu, C. Wang, L. Song, Z. Niu, J. Chen, *Angew. Chem. Int. Ed.* **2019**, *58*, 7062–7067.
- [8] a) Y. Lu, Z. Li, Z. Bai, H. Mi, C. Ji, H. Pang, C. Yu, J. Qiu, *Nano Energy* **2019**, *66*, 104132; b) D. Qiu, J. Guan, M. Li, C. Kang, J. Wei, Y. Li, Z. Xie, F. Wang, R. Yang, *Adv. Funct. Mater.* **2019**, *29*, 1903496; c) R. Yuksel, O. Buyukcakir, P. K. Panda, S. H. Lee, Y. Jiang, D. Singh, S. Hansen, R. Adelung, Y. K. Mishra, R. Ahuja, R. S. Ruoff, *Adv. Funct. Mater.* **2020**, *30*, 1909725; d) Y.-G. Lee, G.-H. An, *ACS Appl. Mater. Interfaces* **2020**, *12*, 41342–41349; e) G.-H. An, *Appl. Surf. Sci.* **2020**, *530*, 147220.
- [9] H. Zhang, Q. Liu, Y. Fang, C. Teng, X. Liu, P. Fang, Y. Tong, X. Lu, *Adv. Mater.* **2019**, *31*, 1904948.
- [10] Z. Li, D. Chen, Y. An, C. Chen, L. Wu, Z. Chen, Y. Sun, X. Zhang, *Energy Storage Mater.* **2020**, *28*, 307–314.
- [11] X. Deng, J. Li, Z. Shan, J. Sha, L. Ma, N. Zhao, *J. Mater. Chem. A* **2020**, *8*, 11617–11625.
- [12] a) M. Kopec, M. Lamson, R. Yuan, C. Tang, M. Kruk, M. Zhong, K. Matyjaszewski, T. Kowalewski, *Prog. Polym. Sci.* **2019**, *92*, 89–134; b) Y. Chen, A. Amiri, J. C. Boyd, M. Naraghi, *Adv. Funct. Mater.* **2019**, *29*, 1901425.
- [13] a) J. Zhao, J. Zhang, W. Yang, B. Chen, Z. Zhao, H. Qiu, S. Dong, X. Zhou, G. Cui, L. Chen, *Nano Energy* **2019**, *57*, 625–634; b) D. Xue, D. Zhu, H. Duan, Z. Wang, Y. Lv, W. Xiong, L. Li, M. Liu, L. Gan, *Chem. Commun.* **2019**, *55*, 11219–11222; c) X.-J. Shen, J.-L. Wen, Q.-Q. Mei, X. Chen, D. Sun, T.-Q. Yuan, R.-C. Sun, *Green Chem.* **2019**, *21*, 275–283.
- [14] a) S. Wang, Z. Zhang, Z. Lu, Z. Xu, *Green Chem.* **2020**, *22*, 4473–4482; b) N. Peeters, K. Binnemans, S. Riano, *Green Chem.* **2020**, *22*, 4210–4221.
- [15] a) H.-F. Yen, Y.-Y. Horng, M.-S. Hu, W.-H. Yang, J.-R. Wen, A. Ganguly, Y. Tai, K.-H. Chen, L.-C. Chen, *Carbon* **2015**, *82*, 124–134; b) D. Wang, T. Liu, J. Wang, Z. Wu, *Carbon* **2018**, *139*, 845–852.
- [16] a) S.-W. Xu, Y.-Q. Zhao, Y.-X. Xu, Q.-H. Chen, G.-Q. Zhang, Q.-Q. Xu, D.-D. Zhao, X. Zhang, C.-L. Xu, *J. Power Sources* **2018**, *401*, 375–385; b) Z. Li, S. Gao, H. Mi, C. Lei, C. Ji, Z. Xie, C. Yu, J. Qiu, *Carbon* **2019**, *149*, 273–280; c) C. Chen, Y. Huang, Z. Meng, M. Lu, Z. Xu, P. Liu, T. Li, *Carbon* **2020**, *170*, 225–235.
- [17] Y. Tian, Y. An, C. Wei, B. Xi, S. Xiong, J. Feng, Y. Qian, *ACS Nano* **2019**, *13*, 11676–11685.
- [18] H. Wang, M. Wang, Y. Tang, *Energy Storage Mater.* **2018**, *13*, 1–7.
- [19] L. Zhang, L. Chen, X. Zhou, Z. Liu, *Adv. Energy Mater.* **2015**, *5*, 1400930.
- [20] S. Chen, L. Ma, K. Zhang, M. Kamruzzaman, C. Zhi, J. A. Zapien, *J. Mater. Chem. A* **2019**, *7*, 7784–7790.
- [21] J. Shi, S. Wang, Q. Wang, X. Chen, X. Du, M. Wang, Y. Zhao, C. Dong, L. Ruan, W. Zeng, *J. Power Sources* **2020**, *446*, 227345.
- [22] L. Chen, Z. Yang, H. Qin, X. Zeng, J. Meng, *J. Power Sources* **2019**, *425*, 162–169.
- [23] H. Sun, L. Mei, J. Liang, Z. Zhao, C. Lee, H. Fei, M. Ding, J. Lau, M. Li, C. Wang, X. Xu, G. Hao, B. Papandrea, I. Shakir, B. Dunn, Y. Huang, X. Duan, *Science* **2017**, *356*, 599–604.
- [24] M. Zhong, H. Liu, M. Wang, Y. W. Zhu, X. Y. Chen, Z. J. Zhang, *J. Power Sources* **2019**, *438*, 226982.
- [25] S. S. Zhang, *Batteries & Supercaps* **2020**, *3*, 1137; *Supercaps* **2020**, *3*, 1137.
- [26] L. Dong, X. Ma, Y. Li, L. Zhao, W. Liu, J. Cheng, C. Xu, B. Li, Q.-H. Yang, F. Kang, *Energy Storage Mater.* **2018**, *13*, 96–102.
- [27] B. Lee, H. R. Seo, H. R. Lee, C. S. Yoon, J. H. Kim, K. Y. Chung, B. W. Cho, S. H. Oh, *ChemSusChem* **2016**, *9*, 2948–2956.

Manuscript received: October 23, 2020

Revised manuscript received: December 28, 2020

Accepted manuscript online: January 5, 2021

Version of record online: March 3, 2021